A98-31470

ICAS-98-1,7,5

PREDICTION OF HIGH-α AERODYNAMIC CHARACTERISTICS OF MANEUVERING AIRCRAFT

M. R. Mendenhall*, S. C. Perkins, Jr.**, and M. C. Hegedus+
Nielsen Engineering & Research
Mountain View, CA USA

ABSTRACT

A physics-based preliminary-design prediction and analysis capability applicable to vehicles in unsteady maneuvers involving nonlinear, time-dependent flow conditions is described. The approach is a direct coupling of fluid dynamics and flight mechanics for use in the flight regimes where the flow phenomena are dominated by vorticity and separation associated with high angles of attack and rapid motions. This method is applicable to generic configurations, it is not dependent on specific empirical information, and it is economical to use. The resulting method, embodied in a computer code called SHAMAN, can be used as a prediction capability for specified vehicle motions or flow conditions, or it can be coupled with a six-degree-of-freedom equation-of-motion solver to predict flight trajectories and transient performance characteristics. Post-stall flight regimes are handled with empirical correlations of wing data. The method is validated by comparison with static and dynamic wind tunnel data on a variety of wing-alone and wing-body configurations.

SYMBOLS

c_n, c_l	section normal force and lift coefficients, respectively
C_l	rolling moment coefficient
C_N	normal force coefficient
p,q,r	roll, pitch, yaw rates
t	time
u,v,w	components of translational velocity
V_∞	free stream velocity
y_{cp}	lateral center of pressure
α	angle of attack
η	semispan position on wing
σ	angle between body centerline and free stream flow vector
Δθ	perturbation angle used in modeling asymmetric vortex separation
Δt	time increment
Γ	vortex strength
ϕ	roll angle, positive right wing down

INTRODUCTION

Modern high-performance fighter aircraft are being designed with maneuverability as a high priority.[1] The vehicle may operate in a flow regime which is characterized by high angles of attack and large angular rotation rates, and the aerodynamic characteristics are dominated by unsteady nonlinear effects induced by flow separation, vortex shedding, and vortex lag effects. During extreme multiple-axis maneuvering conditions, the dynamic and time-dependent effects of these nonlinear flow characteristics contribute significantly to the behavior and maneuvering capability of the aircraft. The presence of the unsteady vortex wake introduces memory into the flow problem, and the nonlinear forces and moments on the vehicle depend on the time history of the motion and the wake development.[2,3,4]

Since many new flight vehicles and concepts are being designed with maneuverability as a high priority, it is essential that analytical methods which can handle dynamic analyses be available early in the design cycle. The prediction methods should correctly represent the physics of the complex flow phenomena associated with rapid maneuvers to predict the time history of the forces and moments, and they should require moderate and reasonable resources to be

* Vice President, Associate Fellow AIAA
**Senior Research Engineer, Member AIAA
+ Research Engineer, Member AIAA

practical and economical in the preliminary design and analysis phase. It is important to emphasize here that the latter requirements dictate an engineering method, not a high-level computational fluid dynamics approach which involves extensive gridding and computer capabilities.

The purpose of this paper is to present recent analytical results for a variety of configurations at high angles of attack. The following section describes briefly some details of the technical approach contained in the prediction method called SHAMAN.[4]

TECHNICAL APPROACH

Maneuvering fighter aircraft motions are characterized by time histories of the translational velocity components (u,v,w) and of the angular rotation rates (p,q,r) around the center of gravity. Extensive wake regions surround the flight vehicle and dominate the induced aerodynamic characteristics as illustrated in Fig. 1. The wake is typically made up of body vortices from the forebody, vortices associated with the wing leading and side edges, and lifting surface trailing vortices.

The unsteady vortex wake causes the flow field to remember previous flow conditions; therefore, vehicle forces and moments depend on the past history of the motion and the wake characteristics. For example, vorticity shed from the nose of the vehicle will pass downstream to influence the loads on the wing and tail surfaces.[5] The vortex-induced loads depend on the motion of the vehicle and the vortex wake during the time it takes the vorticity to be transported from the nose to the tail.[6,7]

A brief outline of the individual flow models required for the analysis is presented in the following sections.

Vortex Wake Model

A key component of the prediction method is the accurate modeling and representation of the forebody and lifting surface trailing vortex field using discrete vortices. The discrete vortex or vortex cloud approach has been used by a number of investigators to successfully predict nonlinear vortex-induced aerodynamics and hydrodynamics for vehicles in steady flows.[8] Of particular relevance to this paper is the capability to model asymmetric vortex separation. References 3 and 7 provide a description of the unsteady vortex cloud method, so the details of this method will not be repeated in this paper.

Static and Dynamic Stall Models

The flow regimes of interest for aircraft maneuvering at high incidence angles will undoubtedly produce stall on the various lifting surfaces. The vortex lattice panel method used to represent the lifting surfaces presumes attached flow; consequently, the predicted loading will exceed the actual loading in the post-stall regime. A stall model which provides reasonable estimates of the loss of loading is needed, but the model should not dominate the computation time. The selected approach is based on empirical corrections to the attached-flow solutions.[4]

Reference 9 presents an extensive survey of flow and wing geometry effects on stall characteristics for low speed flows. Maximum section lift on two dimensional airfoils is shown to be a function of section thickness, leading-edge radius, Reynolds number, and Mach number. For rectangular wings, the centerline section stalls at a value less than the 2-D value for the same airfoil section and Reynolds number, and the maximum section lift varies across the span. As the sweep of the wing leading edge increases, the spanwise variation of maximum section lift becomes more pronounced. For wings with highly-swept leading edges, there is a strong variation of maximum section lift across the span. The inboard and outboard sections have a substantially higher and lower maximum section lift, respectively, than a 2-D airfoil with the same section geometry and Reynolds number. For example, the variation of section lift coefficient with angle of attack at a number of spanwise stations is presented in Fig. 2 for a wing alone configuration with a leading-edge sweep angle of 63 degrees and a maximum thickness of 5%. Note that the maximum section lift coefficient at the root for a 2-D airfoil at the same Reynolds number and with similar geometric characteristics is 0.9.

The stall model contained in SHAMAN requires that the spanwise variation of maximum section normal force coefficient and a generic description of the post-stall normal force behavior be specified. This information can be obtained from sources such as Reference 9, experimental data, or CFD calculations. In the application of the stall model, the attached-flow section normal force at each spanwise station on the lifting surface is compared with the maximum section

loading as derived from the stall model. If the predicted normal force is greater than that indicated by the stall model, the predicted value is reduced to agree with the section data at an equivalent angle of attack. This correction procedure is applied to each spanwise section of the lifting surface. The bound and trailing leg strengths on the surface are adjusted to match the correct loading, and these modified strengths define the lifting surface wake.

An aircraft undergoing rapid maneuvers at high angles of attack will experience the phenomenon of dynamic stall (or dynamic lift); that is, the higher than expected lift generated on a wing pitching to an angle well beyond the static stall angle. This is a critical phenomenon which must be included in the flow model for accurate prediction of maneuvering aerodynamic characteristics. An empirical correlation model similar to that used for the static stall model was selected using wing data for positive pitch rates[10] and negative pitch rates.[11] Correlations were developed for correction factors which are a function of pitch rate and Mach number. The factors modify the value of maximum c_n at the end of the linear range and account for the shape of the normal force curve in the post-stall regime. This empirically based model, while obviously not definitive for all configurations, provides a reasonable means for estimating the dynamic overshoot and undershoot of normal force which can be encountered during rapid, high-α maneuvers.

Vortex Breakdown

The aerodynamic characteristics of highly swept delta wings are dominated by two leading edge vortices which form over the suction surface of the wing. The angle of attack at which these vortices first form is primarily a function of the wing sweep angle. These vortices are responsible for the high lift achieved by delta wings at high angles of attack. In SHAMAN, this effect is modeled using the Polhamus suction analogy[9]. At sufficiently high angles of attack, these vortices undergo a transition known as vortex breakdown or vortex burst. Breakdown first occurs near the trailing edge, then moves forward toward the apex with increasing incidence. After reaching the apex, a further increase in incidence results in the loss of a coherent vortex field over the wing.

Vortex burst has been reported[12] to be a function of a large number of geometric and flow parameters, as well as testing techniques, and as such, there is no definitive set of vortex burst data for delta wings. Within SHAMAN, the travel of the vortex burst location is specified by the relationships defined in Ref. 13. These relationships appear to provide a reasonable overall estimate of vortex burst location on delta wings alone for a wide range of sweep angles, although comparisons with certain data sets indicate poor agreement between predicted and measured locations. In the application of vortex burst effects in SHAMAN, the calculated axial location of burst on the wing determines the spanwise location outboard of which leading-edge suction effects are not included. However, it has been found that a residual vortex lift exists on regions of the wing aft of the burst location.[13] In other words, the lift on the wing is larger than that given by the potential loading. To account for this residual vortex loading, correlations of the variation of a residual factor which is a function of burst location and leading-edge sweep angle are included in SHAMAN.

Trajectory Simulations

The prediction method can be used for unsteady trajectory simulations in two distinct ways. First, the vehicle motion can be calculated by integrating the six-degrees-of-freedom equations-of-motion with a direct simulation approach. This method does not require a priori knowledge of the vehicle stability derivatives; instead, the method accepts the instantaneous forces and moments on the vehicle as provided by the analysis to produce the translational and rotational accelerations at the specified time. The three forces and three moments, including apparent mass effects, become the right-hand side of the six equations of motion. Integration over a specified Δt produces the translational and angular velocities which can be integrated to determine the position and attitude of the vehicle. This approach has been successful in wing-rock prediction of fighter aircraft models[3,4] and maneuvering trajectories of submarines.[7]

Similarly, the method can also be used in an unsteady calculation by specifying the motion of the vehicle as a function of time. For example, the unsteady flight conditions of a model undergoing forced oscillations in a tow-tank test were replicated.[2] This technique has also been used to model the trajectories of an aircraft in flight tests to examine the resulting flow field associated with the motions.[4] This approach has

the advantage of allowing the detailed study of the unsteady wake and aircraft loads associated with a specific maneuver without the details and problems involved with trying to predict a specific trajectory. This latter approach proved useful in the investigation of a departure flight condition described in References 4 and 14.

Aerodynamic Design and Analysis Method

A physics-based, engineering prediction method (SHAMAN) applicable to the unsteady and nonlinear flow conditions associated with maneuvering flight vehicles at high angles of incidence and high rotation rates is described.[3,4] Key elements of the prediction method are (1) the accurate modeling and representation of the forebody and lifting surface trailing vortex field using discrete vortices, (2) static and dynamic stall models to represent the lifting surface loadings at the high angles of attack of interest, and (3) a trajectory simulation capability which can represent a typical fighter maneuver and exhibit the complex flow fields during the motion. The applicability of the method to preliminary design is dictated by the ease of use of the method and the quality of the results for a wide range of configurations in a variety of flight conditions.

The technical approach described has practical application to preliminary design studies of maneuvering vehicles prior to wind tunnel or flight testing, and it also has application at a number of levels during the design of a modern flight vehicle. Beginning in the concept phase, the method can be used to predict the static aerodynamic characteristics of the configuration at high angles of attack in the post-stall flight regime. It can also be used to investigate maneuvering flight characteristics during this early stage of the design. As the design evolves and more information on the aerodynamic characteristics of the vehicle becomes available, either through wind tunnel testing or advanced computational fluid dynamics, the method can be updated and improved with this information. At even later stages of the design, after flight testing for example, the full-scale aerodynamics can be used to further update and improve the flow models in the method. The method can then be used for analytical simulations outside the normal flight envelope for investigations into these unknown flight regimes with greater safety.

The SHAMAN code, which contains the prediction method described above, has the necessary attributes for a preliminary design method. It requires only a few hours to set up a new configuration from preliminary geometry files, and modifications to the geometry for design changes or parametric studies are accomplished in a very short time. Set-up times for typical steady and unsteady runs on a work station are also short. Individual run times for steady runs at a single flow condition require only a few minutes. Unsteady runs for long maneuvering trajectories can require several hours depending on the complexity of the configuration and the length of the maneuver.

An interactive graphical interface assists in the input preparation by combining user-specified modules for a specific configuration and supplying graphical feedback of the aerodynamic model geometry for comparison with the original CAD geometry files. The geometry displays change dynamically during the input preparation to assist the user in accurate geometry specification. This tool has proved a valuable time-saving device during the setup of preliminary configurations for initial high-angle-of-attack or trajectory simulations.

RESULTS

A variety of results are available to demonstrate the prediction method. The discussion in this section will try to cover a wide variety of configurations to demonstrate the use and capability of the method. Beginning with simple wing-alone configurations and progressing through more complex wing-body configurations, the results will show the predicted aerodynamic characteristics in the post-stall regime and illustrate the strengths and weaknesses of the high-alpha capabilities of the method.

Static

The first wing-alone configuration is a rectangular wing with aspect ratio 5 which was tested to $\alpha = 90°$ as shown in Fig. 3.[15] Experimental data on a similar wing tested to stall is also shown in this figure.[16] The predicted results shown by the dashed curve are the unstalled aerodynamic characteristics, and those represented by the solid curve are obtained with the SHAMAN stall model implemented. Though some of the details are missing in the post-stall regime, the general characteristics of the predicted normal force

coefficient are in reasonable agreement with the experiments.

Measured and predicted normal force and center of pressure results on a 65-deg. delta wing are compared in Figs. 4 (a) and (b). Three different sets of experimental data on similar wings are shown in this figure.[17,18,19] The predicted curves are shown for two different runs. The dashed curve is for an unstalled wing with no leading-edge vortex breakdown considered. The solid curve represents the predicted results on the wing with both the stall model and leading-edge vortex breakdown effects included. The estimated angles of attack at which the vortex breakdown crosses the trailing edge (T.E.) and reaches the apex are shown by the arrows on the α-axis. In general, the normal force is predicted within the scatter in the experimental data. There is significantly more scatter in the center of pressure data in Fig. 4(b), but the predicted results are not unreasonable.

The same 65-deg. delta wing was also tested at different roll angles at high angles of attack.[18,20] The wing was rolled around its axis while at constant 30-deg. angle of attack, and a set of representative results for normal force are shown in Fig. 5. Notice that the data from Ref. 18 are only for zero roll angle, but they are shown to illustrate some difference which may be caused by the test rig. The predicted results from SHAMAN exhibit the correct trend, but the level of the predicted normal force as a function of roll angle is approximately 10% lower than the measurements. This is comparable to the difference in measured and predicted normal force at zero roll angle.

Measured and predicted spanwise distributions of normal force on a 63-deg. delta wing are shown in Fig. 6. The data[21,22] are from pressure measurements on the wings. Notice that there is only a small influence from the fuselage in Ref. 22. The predicted results are from SHAMAN with the stall and breakdown models included. The general agreement is very good, although the predicted loading is slightly lower than the measurements on the inboard portion of the wing.

The next configuration considered is the generalized fighter model tested by NASA Langley Research Center.[23] This wing-body configuration has a moderate sweep angle such that there are no significant leading-edge vortices in the flow field to influence the aerodynamic characteristics. Unpublished experimental data on this model with a circular cross section fuselage were made available for this work.[24] Measured and predicted normal force coefficients on the model up to $\alpha = 50°$ are shown in Fig. 7(a). As before, the predicted results with wing stall effects included are shown by the solid curve. Agreement with the measurements is very good up to approximately 40 deg. Note that all predicted results shown in Fig. 7(a) were obtained using a calculated symmetric (about the vertical plane of symmetry) vortex field. At higher angles of attack the vortex field will be asymmetric, and the use of such a modeled vortex field will reduce the predicted value of C_N.

In this regard, rolling moment data[24] for $\sigma = 35°$ were used for the purpose of calibrating an asymmetric vortex field model. This is done by perturbing the circumferential location of the separation points on the forebody by a specified amount ($\Delta\theta$). The measured and predicted rolling moments on the generalized fighter configuration at $\sigma = 35°$ are compared in Fig. 7(b) where the results are in reasonable agreement for roll angles less than 30 deg. The trend of the data is predicted well up to $|\phi| \approx 30°$, but the magnitude of C_l is overestimated in this region. The irregular behavior of the data at larger roll angles is not understood at this time, but it is likely due to interference effects associated with the asymmetric forebody vortex field as each wing passes through the field. Note that both the data and the predicted results indicate a change in slope ($\Delta C_l/\Delta\phi$) starting at $|\phi| \approx 30°$; however, the nearly-constant C_l in the region $30° < |\phi| < 45°$ is not predicted. Note, however, that the difference between measured and predicted C_l at $\phi = 30°$ is represented by an outboard shift of y_{cp} of the predicted potential load on the right wing by a mere 3.5% of the exposed span! This is indicative of the sensitivity of the prediction in this vortex-dominated region. Additional experimental data, such as C_N and C_Y as a function of ϕ, were not available, but might have provided insight into the source of the differences between measured and predicted variation of C_l with ϕ.

Unsteady

The aforementioned generalized fighter model exhibited limit cycle wing rock motion in a wind tunnel.[23] Similar unpublished data[24] from NASA/Langely Research Center for a circular cross

section forebody are shown in Fig. 8 for $\sigma = 35°$. These data exhibit wing rock with amplitude of approximately 30 degrees at a frequency of 0.5 Hz.

Using the asymmetric vortex model developed from static test data, the resulting predicted wing rock motion and the rolling moment coefficients are shown in Figure 9. The roughness in the rolling moments is caused by the sensitivity of the vortex-induced effects on the wing represented by finite panels. The predicted amplitude is approximately 18 degrees at 1 Hz. The difference between measured and predicted amplitude is likely due to the larger predicted C_l than that indicated by the static data for the region $|\phi| < 30°$. This is especially true for the left-wing-down comparisons (i.e., $-\phi$), where the predicted C_l is considerably higher than the data. The larger-than-measured predicted restoring moment apparently overcomes inertial effects at roll angles which are less than those experienced in the wind tunnel test, resulting in a wing rock which is smaller in amplitude and higher in frequency. It is worth noting that the asymmetric vortex model assumes the same magnitude of perturbation angle ($\Delta\theta$) for $+\phi$ and $-\phi$, thereby resulting in an antisymmetric variation of C_l vs ϕ. However, the data do not exhibit this same perfectly antisymmetric variation. This suggests that an asymmetric vortex model which uses different magnitudes of $\Delta\theta$ for $+\phi$ and $-\phi$ flow conditions may be appropriate for this case. If the magnitude of the predicted static rolling moments was reduced for the region $-30° < \phi < 0°$, it is likely that the configuration would roll beyond $\phi = -20°$ and would exhibit wing rock with larger amplitude and lower frequency than shown in Fig. 9. Additionally, the predicted result could be improved if more accurate information on the inertial characteristics of the model and rolling friction in the model support mechanism were known.

Note that unsteady results for an X-31 fighter configuration have previously been presented in Ref. 14. In this reference, predicted wing rock results for a small-scale model of an X-31 are presented, along with comparisons of flight test and predicted time histories of aerodynamic characteristics for a full-scale X-31 undergoing pitch-up and departure maneuvers.

CONCLUSIONS

The application of a physics-based prediction method to predict the nonlinear behavior of typical flight vehicles in unsteady flows is described. An important feature of the prediction method is the accurate modeling of the complex vortex wake flow field in the vicinity of the vehicle. Knowledge of the time history of the vortex wake associated with the vehicle motion is an essential part of the total flow model and prediction method.

ACKNOWLEDGMENTS

The authors acknowledge DARPA for support of the high-α fighter analysis and the development of SHAMAN. Dr. Michael S. Francis was the original technical monitor for this effort, and his contributions through numerous technical discussions are greatly appreciated. Dr. James McMichael is the current technical monitor, and the authors appreciate his interest in the project and his helpful discussions.

REFERENCES

1. Lang, J. and Francis, M. S.: Unsteady Aerodynamics and Dynamic Aircraft Maneuverability. AGARD-CP-386, May 1985.

2. Mendenhall, M. R. and Perkins, S. C., Jr.: Analysis of Dynamic Maneuver Performance of Fighter Aircraft at High Angles of Attack. AFWAL-TR-88-3048, July 1988.

3. Mendenhall, M. R., Perkins, S. C., Jr., and Ericsson, L. E.: Prediction of Forebody Vortex-Induced Wing Rock on Wing-Body Configurations. AIAA 93-3451, Aug. 1993.

4. Mendenhall, M. R. and Perkins, S. C., Jr.: Computational Methodology for Maneuvering Aircraft at High Angles of Attack. NEAR TR 508, Mar. 1996.

5. Mendenhall, M. R., Perkins, S. C., Jr., and Lesieutre, D. J.: Prediction of the Nonlinear Aerodynamic Characteristics of Maneuvering Missiles. Journal of Spacecraft and Rockets, Vol. 24, Sept.-Oct. 1987, pp. 394-402.

6. Mendenhall, M. R. and Perkins, S. C., Jr.: An Unsteady Vortex Wake Model for Maneuvering Vehicles. AGARD Symposium on The Characteristics & Modification of

Wakes from Lifting Vehicles in Fluids, Trondheim, Norway, May 1996.

7. Mendenhall, M. R. and Perkins, S. C., Jr.: Prediction of Vortex-Induced Fluid Mechanics of Maneuvering Submarines. AIAA 93-0638, Jan. 1993.

8. Mendenhall, M. R., Perkins, S. C., Jr., and Lesieutre, D. J.: Vortex Cloud Model for Body Vortices and Tracking. Tactical Missile Aerodynamics: Prediction Methodology, Vol. 142 of Progress in Astronautics and Aeronautics, ed. by M. R. Mendenhall, AIAA, 1992, pp. 225-285.

9. Polhamus, E. C.: A Survey of Reynolds Number and Wing Geometry Effects on Lift Characteristics in the Low Speed Stall Range. NASA CR-4745, June 1996.

10. Carr, L.W. and Chandrasekhara, M. S.: An Assessment of the Impact of Compressibility on Dynamic Stall. AIAA 95-0779, Jan. 1995.

11. Niven, A. J. and Galbraith, R. A. McD.: Experiments on the Establishment of Fully Attached Airfoil Flow from the Fully Stalled Condition During Ramp-Down Motions. ICAS Paper 90-3.4.3, Sept. 1990.

12. Nelson, R. C. and Thompson, S. A.: The Unsteady Aerodynamics of a Delta Wing Undergoing Large Amplitude Pitching Motions. PhD. Dissertation, Department of Aerospace and Mechanical Engineering, University of Notre Dame, Apr. 1992.

13. Huang, X. Z. and Hanff, E. S.: Prediction of Normal Force on a Delta Wing Rolling at High Incidence. AIAA 93-3686, Aug. 1993.

14. Mendenhall, M. R. and Perkins, S. C., Jr.: Predicted High-α Aerodynamic Characteristics of Maneuvering Aircraft. AIAA 96-2433, June 1996.

15. Wieselsberger, C. and Betz, A.: Ergebnisse der Aerodynamischen Versuchsanstalt zu Goottingen. Pub. by Druck und Verlag von R. Oldenbourg, 1921.

16. Holme, O. A. M.: Measurements of the Pressure Distribution on Rectangular Wings of Different Aspect Ratios. Aeronautical Research Institute of Sweden Report No. 37, 1950.

17. Wentz, W. H., Jr. and Kohlman, D. L.: Wind Tunnel Investigations of Vortex Breakdown on Slender Sharp-Edged Wings. NASA CR 98737, Nov. 1968.

18. Unpublished data, joint Air Force Research Laboratory/Canadian Institute for Aerospace Research test program, 1993. Furnished by Dr. Deborah S. Grismer, 1998.

19. Jarrah, M-A. M.: Unsteady Aerodynamics of Delta Wings Performing Maneuvers to High Angles of Attack. Ph.D. Thesis, Dept. of Aeronautics and Astronautics, Stanford University, Dec. 1988.

20. Huang, X. Z. and Hanff, E. S.: Prediction of Leading-Edge Vortex Breakdown on a Delta Wing Oscillating in Roll. AIAA 92-2677, June 1992.

21. Anderson, A. E.: Chordwise and Spanwise Loadings Measured at Low Speed on Large Triangular Wings. NACA RM A9B17, Apr. 1949.

22. Kolbe, C. D. and Boltz, F. W.: The Forces and Pressure Distribution at Subsonic Speeds on a Plane Wing Having 45^0 of Sweepback, an Aspect Ratio of 3, and a Taper Ratio of 0.5. NACA RM A51L21, Oct. 1951.

23. Brandon, J. M. and Nguyen, L. T.: Experimental Study of Effects of Forebody Geometry on High Angle of Attack Static and Dynamic Stability. Journal of Aircraft, Vol. 25, No. 7, July 1988, pp. 591-597.

24. Private Communication with J. M. Brandon of the NASA Langley Research Center.

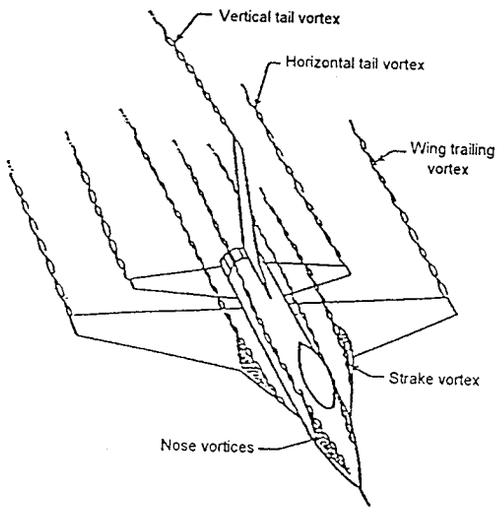

Fig. 1.- Sketch of the flow field around a maneuvering aircraft at high angles of attack.

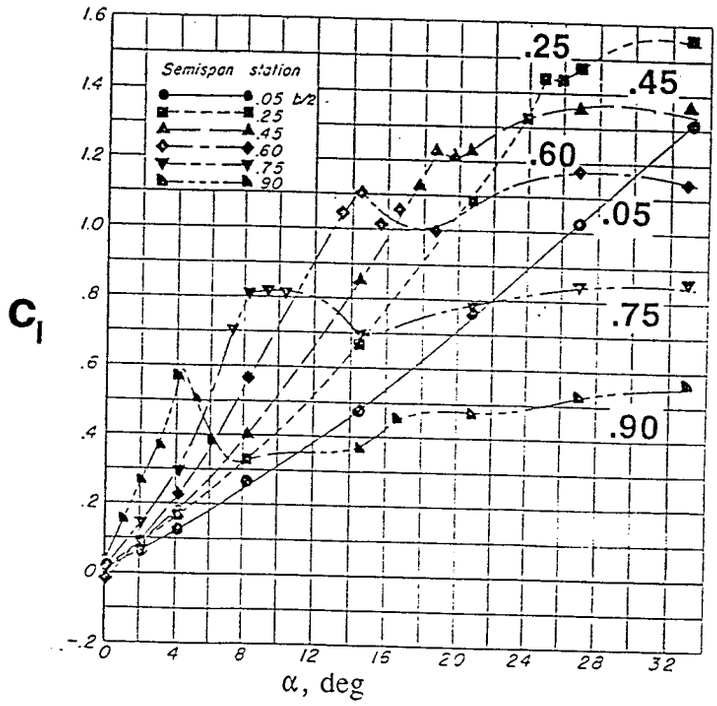

Fig. 2.- Measured variation of section lift coefficient with angle of attack for a 63-deg. delta wing.

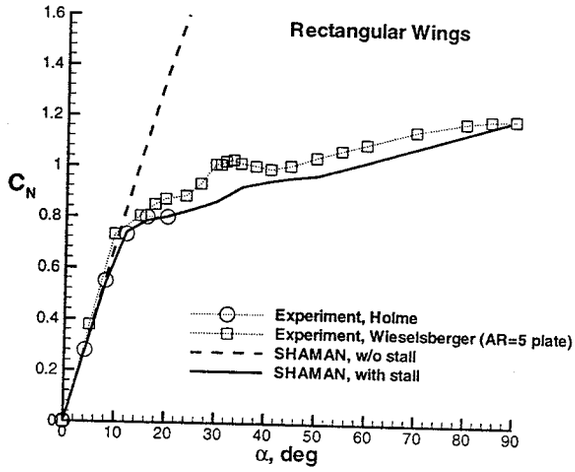

Fig. 3.- Measured and predicted normal force on a rectangular wing at high angles of attack.

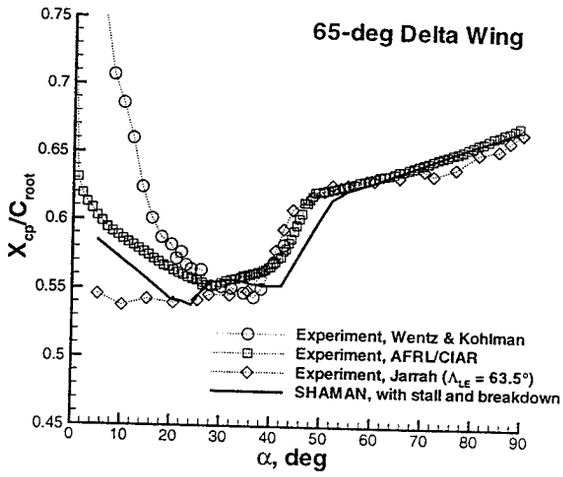

(b) Axial center of pressure

Fig. 4.- Concluded.

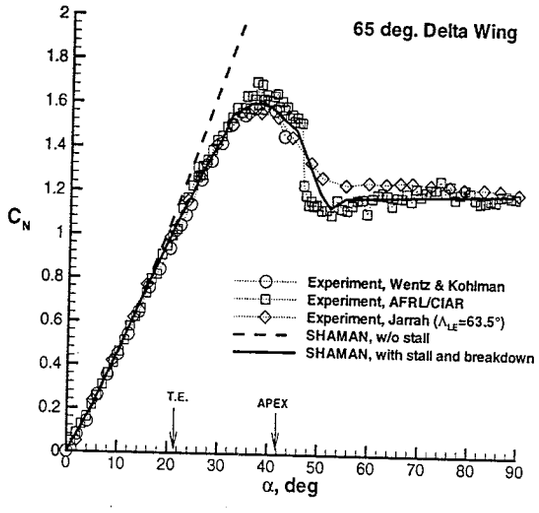

(a) Normal force coefficient

Fig. 4.- Measured and predicted aerodynamic characteristics of a 65-deg. delta wing at high angles of attack.

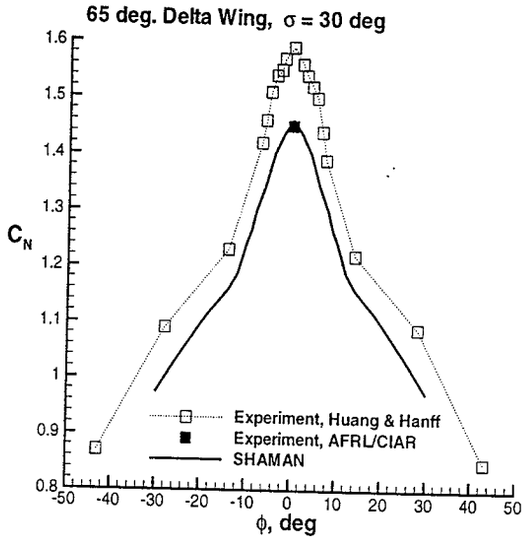

Fig. 5.- Measured and predicted normal force on a rolled 65-deg. delta wing at σ = 30°.

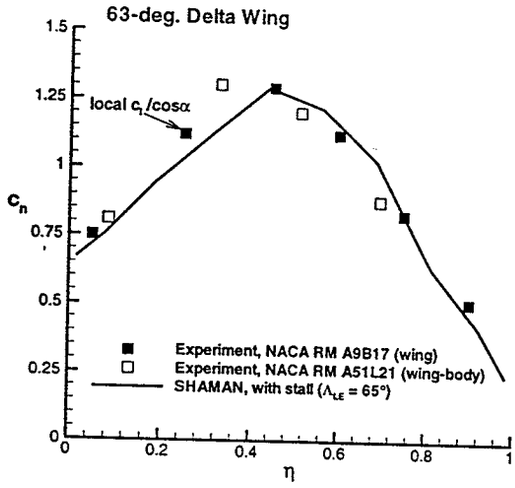

Fig. 6.- Measured and predicted spanload distribution on a 63-deg. delta wing at $\alpha = 20°$.

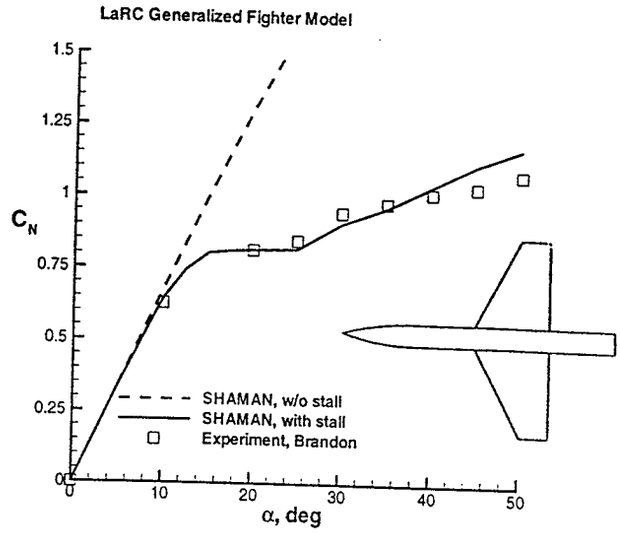

(a) Normal force coefficient

Fig. 7.- Measured and predicted aerodynamic characteristics for a generalized fighter model at high angles of attack.

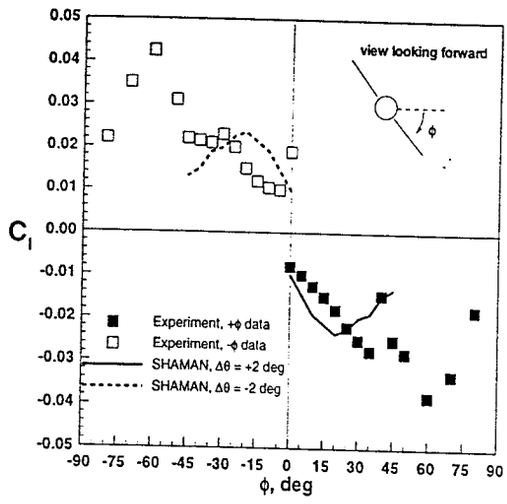

(b) Rolling moment coefficient, $\sigma = 35°$.

Fig. 7.- Concluded.

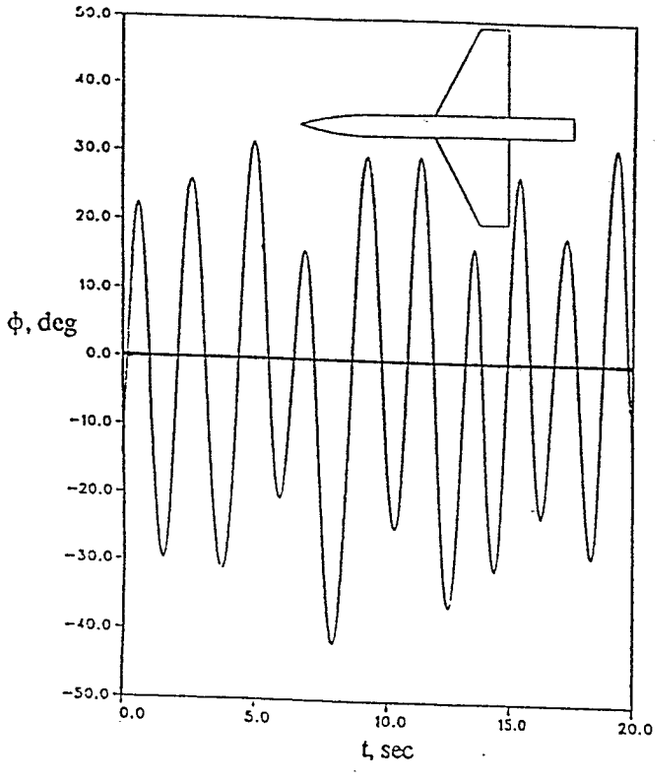

Fig. 8- Measured wing rock on a generalized fighter model, $\sigma = 35°$.

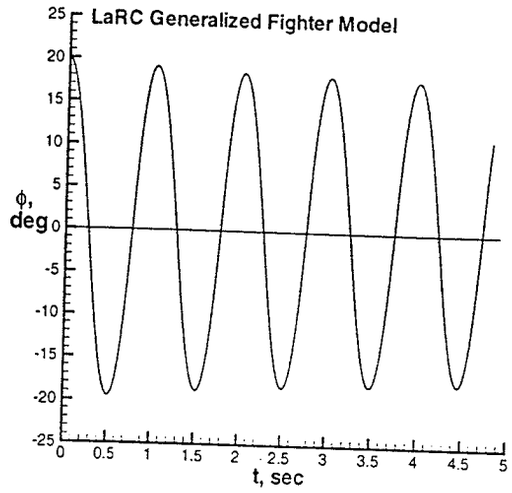

(a) Roll angle time history

Fig. 9.- Predicted wing rock on a generalized fighter model, $\sigma = 35°$.

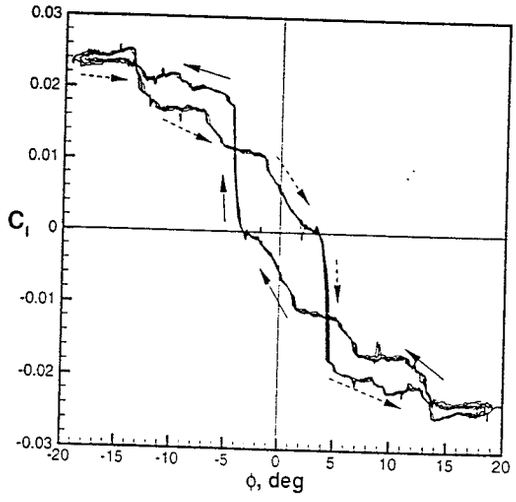

(b) Rolling moment coefficient

Fig. 9.- Concluded.